Damage Process Modeling on SMC

JOSEF KABELKA, LEO HOFFMANN, and GOTTFRIED W. EHRENSTEIN*

Chair for Polymer Technology, Center for Composites, University of Erlangen-Nuremberg, Germany

SYNOPSIS

The damage processes taking place in SMC, which has been subjected to monotonically increasing tensile loads, are analyzed and the stress-strain curves are calculated. SMC is viewed as a laminate consisting of fiber bundles embedded in a resin/filler matrix. The stiffness of bundles and matrix is expected to be influenced by developing cracks, which lead to a reduction of the total stiffness of the SMC. Crack creation, and consequent bundle and matrix stiffness reduction, are viewed as a statistical process. The quadratic criterion in stress space and the maximum strain criterion are used to predict failure in the fiber bundles and in the matrix, respectively. Residual stresses resulting from the high curing temperatures, anisotropic fiber orientation, and varying content of filler particles in the matrix, inside and outside of the fiber bundles, are taken into account. The comparison of predicted stress-strain curves to experimental results, obtained on almost 20 different SMC materials, shows very good agreement, especially at elongations less than 1%. The model developed in this work allows us to appreciate quantitatively the influence of different material and processing parameters on the behavior of SMC, and in this way, to optimize its composition. © 1996 John Wiley & Sons, Inc.

INTRODUCTION

Due to its heterogeneous composition, sheet molding compound (SMC) is a very damage-sensitive material. Basically, it is a preimpregnated polyester resin reinforced by short, randomly distributed glass fibers. Various components are added to the resin in order to achieve properties that facilitate subsequent processing and are desirable in the finished products. Possible additives include: accelerators, fillers, thickeners, shrinkage compensators, pigments, flame retardants, and light stabilizers.

A typical undesirable feature of the SMC structure is that the glass rovings, applied during the fabrication of the SMC structure, do not disintegrate into individual fibers after they have traveled through a cutter. Instead, flat fiberglass bundles, most of which are oriented parallel to the direction of the take-up belt, are formed and behave as effective reinforcing agents (Fig. 1). The tightly packed fiber bundles act like a sieve, preventing larger filler particles from penetrating into the internal bundle space. Therefore, the particle distribution throughout the matrix can be considerably nonhomogeneous. To simplify the analysis of the SMC structure, it can be viewed as an aggregate of microlaminae stacked one upon the other. Then the uniform strain concept, under in-plane loading, can be used in conjuction with the laminate analogy[1] to analyze the SMC structure.

The properties of the SMC structure are determined by its material composition and the properties of each constituent, as well as by the processing parameters. A major problem, which occurs when working with SMC, is the buildup of residual stresses. Significant residual stresses occur in the SMC structure during process cooling, due to the high curing temperatures and a mismatch in thermoelastic properties between fibers, resin, and filler. Cooling generates local transverse tensile stresses in fiber bundles and the matrix, which surrounds the fibers, resulting in considerable local reduction of the load bearing capacity and can significantly contribute to the initiation of microcracking at ambient conditions. The influence of individual structural, material, and processing parameters on the

* To whom correspondence should be addressed.

Journal of Applied Polymer Science, Vol. 62, 181-198 (1996)
 CCC 0021-8995/96/010181-18

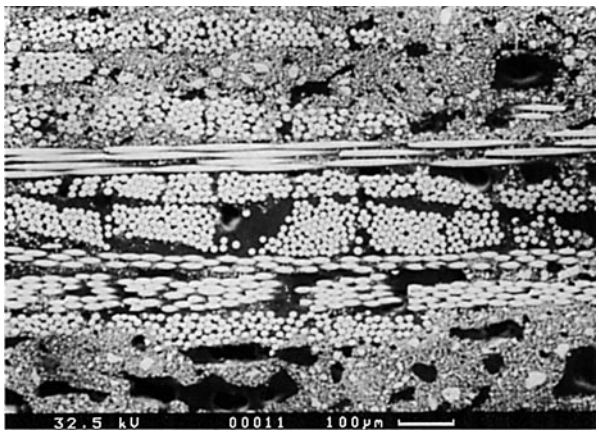

Figure 1 Typical SMC structure.

degradation of the SMC properties, under a monotonically increasing tensile load, is examined in this article.

MATHEMATICAL MODEL

SMC is viewed as a multilayer composite material consisting of identical layers. It is assumed that the individual layers are void free and adhere firmly to one another. For volume fractions (v) of individual components, resin compound (r), filler (p) and fiber (f), the following applies:

$$v_r + v_p + v_f = 1$$

INITIAL THERMOELASTIC PROPERTIES

The fundamental element of the SMC structure is the fiber bundle saturated by a matrix. This matrix (resin/filler mixture) will be referred to as the "internal" matrix, which is assumed to be isotropic with elastic properties E_{mi}, ν_{mi} and α_{mi}. Each fiber bundle represents a unidirectional (UD) layer. The thermoelastic parameters (TEP), which include the moduli E_L, E_T, G_{LT}, G_{TT}, Poisson's ratios ν_{LT}, ν_{TT}, and thermal expansion coefficients α_L, α_T, can be calculated in terms of the TEP of fibers and matrix using the formulae by Hashin.[2] Where the subscripts L and T signify the longitudinal and transversal directions, repectively, with respect to the fiber bundles. By examining polished sections of SMC specimens, it was determined that the fiberglass fraction, Φ_f, in the fiber bundle was about 50% by volume. Thus, it was determined that the bundle volume fraction of the SMC structure (Φ_b) is equal to $2v_f$.

The TEP of the matrix can be calculated by combining the formulae of Kerner and Hashin[1] or by using the "S-combining-Rule,"[4] when an isotropic and roughly spherical filler (e.g., calcium hydrate) is used. If the filler particles are uniformly distributed throughout the whole volume of SMC, the filler fraction Φ_{pu} in the matrix (resin/filler mixture) is $\Phi_{pu} = v_p(v_r + v_p)^{-1}$. Due to a "sieve effect" of the fiber bundles, the filler fraction in the internal bundle space, Φ_{pi}, can be smaller than that in the matrix (referred to as "external" matrix) surrounding the bundles, Φ_{pe}. That is, $0 \leq \Phi_{pi} \leq \Phi_{pu}$. The following relation exists between Φ_{pi} and Φ_{pe}:

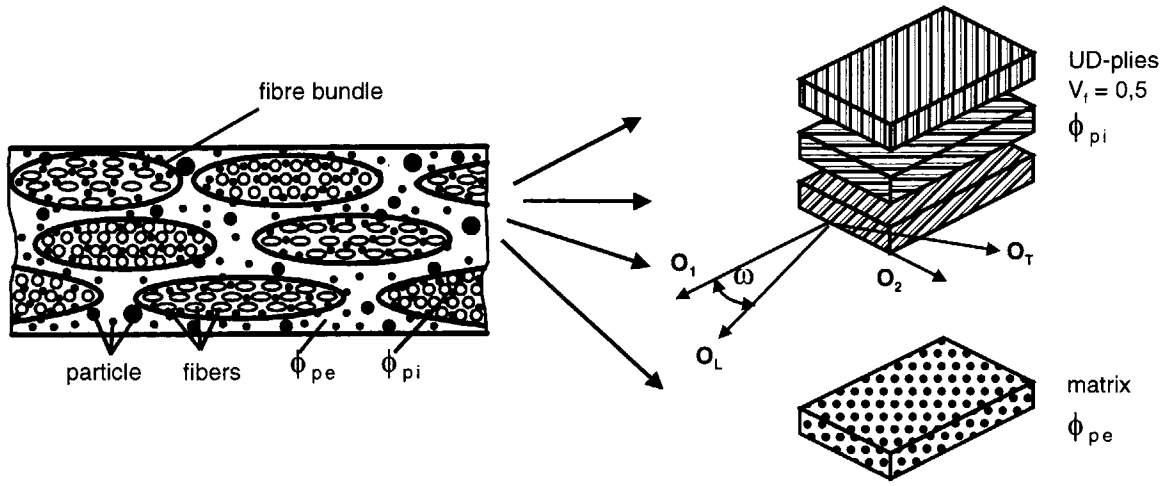

Figure 2 Representation of SMC by means of a multilayer composite consisting of UD plies. Designation of the coordination system.

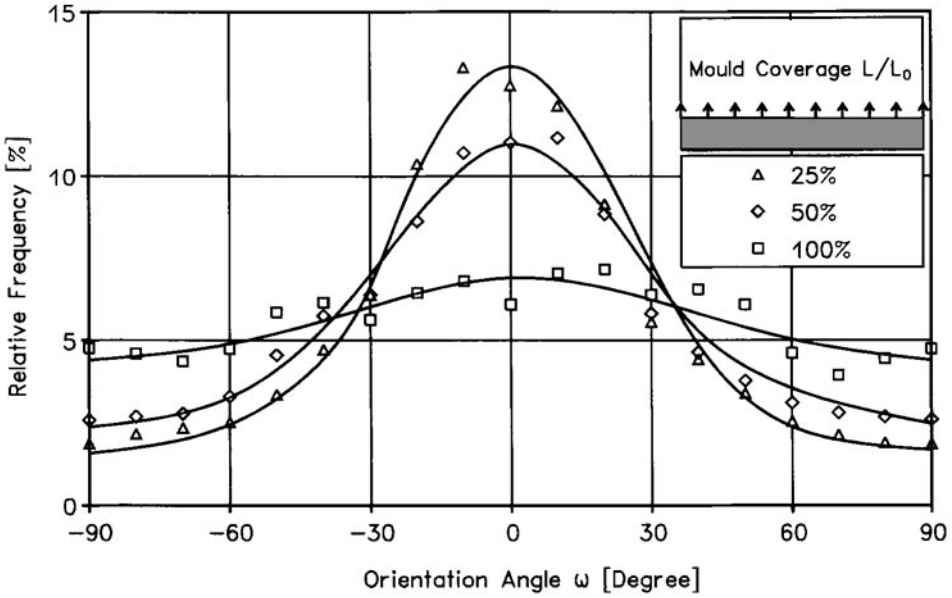

Figure 3 Plots of the distribution function $H(\omega)$ for different molding charges.[16]

$$\Phi_{pe} = \frac{v_p - \Phi_{pi} v_f}{v_p + v_r - v_f} \tag{1}$$

On the basis of the TEPs of the resin compound, filler, and the filler fractions Φ_{pi} and Φ_{pe}, the TEPs of the "internal" (e.g., E_{mi}, ν_{mi}, and α_{mi}) as well as of the "external" (e.g., E_{me}, ν_{me}, and α_{me}) matrices can be calculated.

The fiber bundles saturated by the "internal" matrix represent effective reinforcing elements and can be understood as "macroscopic" fibers with anisotropic properties, embedded in the "external" matrix. The bundles are randomly distributed throughout the SMC and oriented in different directions with respect to the global coordinate system defined by 0_1 and 0_2 axes, as shown in Figure 2. Collecting all the bundles that lie in the same direction into one ply, the stochastic laminate structure is transformed into a multilayer composition. This composition, consisting of a great number of UD

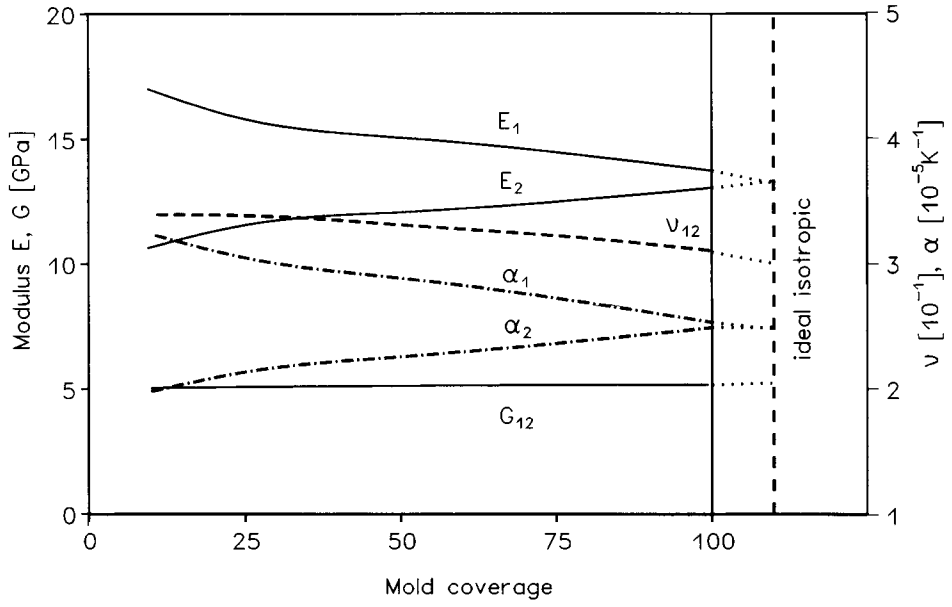

Figure 4 Initial moduli and thermal expansion coefficients of SMC as functions of mold coverage.

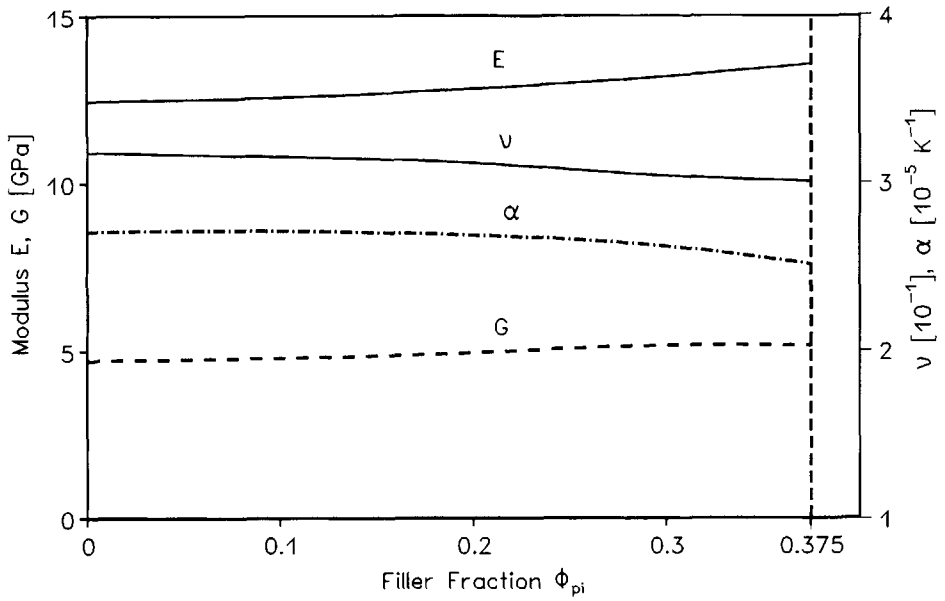

Figure 5 Initial thermoelastic properties of SMC as functions of the filler fraction Φ_{pi}.

plies with identical properties, also includes a layer representing the "external" matrix. Stiffness matrix elements of a UD ply, defined in its local coordinate system by the 0_L and 0_T axes, can be calculated on the basis of Φ_f, TEPs of the "internal" matrix and of the fibers. The stiffness matrix of the total laminate is then determined by summing up the stiffnesses of individual layers in the directions of the global coordinate axes, 0_1 and 0_2. The stiffnesses of the UD plies, which are functions of the orientation angle ω, are obtained by means of well-known transformation formulae (e.g., [5]).

In the case where the bundle distribution is nonuniform with respect to the orientation angle ω, a specific bundle alignment exists and is described by a distribution function $H(\omega)$. The elements of the laminate initial stiffness matrix (C_{ijo}) can be obtained from the following:

$$\overline{C_{ijo}} = \frac{1}{\pi} \int_{-\pi/2}^{\pi/2} H(\omega) C_{ijo}(\omega)\, d\omega \qquad (2)$$

The distribution function $H(\omega)$ is used with regard to the results of Starke and Michaeli[16] in the following form:

$$H(\omega) = C + Ae^{-B\omega^2} \qquad (3)$$

where A, B, and C are constants. Starke and Michaeli[16] achieved different degrees of fiber orientation, between experiments, by varying the size of the mold charge coverage area within a square mold. The fiber alignment, developed in these experimental cases, was a result of the one-dimensional flow the charge underwent in the square mold.

The fiber orientation function $H(\omega)$ is symmetric to the 0_1-axis, where the orientation angle ω is 0°. The case of B = 0 relates to the uniform distribution of bundles; the SMC is planar isotropic. The material properties become orthotropic with extreme values of $\omega = 0°$ and $\omega = 90°$, and when $B > 0$. Plots of $H(\omega)$, for various mold coverages, are presented in Figure 3. It can be seen that some bundle alignment is already present in the material at the virgin state; in this instance, no material flow had occurred during processing due to a 100% mold coverage.

The integration shown in eq. (2) is only possible numerically. When the stiffness matrix elements are determined, elastic moduli of the SMC in the direction of its orthotropic axes, 0_1 and 0_2, can be calculated using the following formulae:

$$\bar{E}_{110} = \bar{C}_{110}\left(1 - \frac{\bar{C}_{120}^2}{\bar{C}_{110}\bar{C}_{220}}\right)$$

$$\bar{E}_{220} = \bar{C}_{220}\left(1 - \frac{\bar{C}_{120}^2}{\bar{C}_{110}\bar{C}_{220}}\right)$$

$$\bar{\nu}_{120} = \frac{\bar{C}_{120}}{\bar{C}_{220}}$$

$$\bar{G}_{120} = \bar{C}_{660} \qquad (4)$$

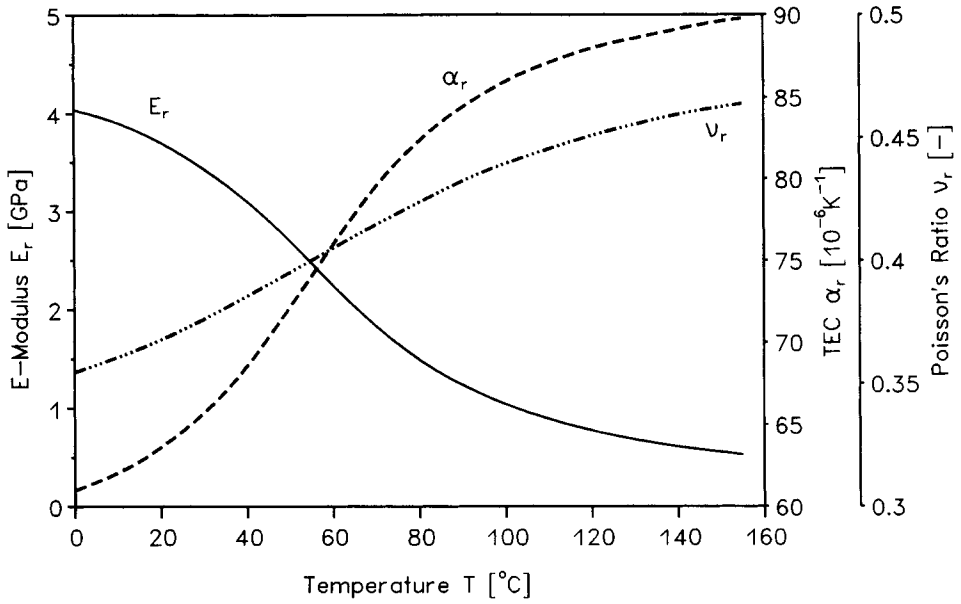

Figure 6 Dependence of thermoelastic properties of the UP resin on temperature.

To determine the thermal expansion coefficients (TEC) of the laminate, the following integrals must be calculated:

$$Q_1 = \frac{1}{\pi} \int_{-\pi/2}^{\pi/2} H(\omega)(C_{120}(\omega)\alpha_{110}(\omega) + C_{220}(\omega)\alpha_{220}(\omega))\, d\omega$$

$$Q_2 = \frac{1}{\pi} \int_{-\pi/2}^{\pi/2} H(\omega)(C_{110}(\omega)\alpha_{110}(\omega) + C_{120}(\omega)\alpha_{220}(\omega))\, d\omega \quad (5)$$

where the transformation formulae for $\alpha_{110}(\omega)$ and $\alpha_{220}(\omega)$ are as follows:

$$\alpha_{110}(\omega) = \alpha_L \cos^2\omega + \alpha_T \sin^2\omega$$

$$\alpha_{220}(\omega) = \alpha_L \sin^2\omega + \alpha_T \cos^2\omega$$

The TECs of the laminate then are

$$\bar{\alpha}_{110} = \frac{1}{D}(Q_1\bar{C}_{120} - Q_2\bar{C}_{220})$$

$$\bar{\alpha}_{220} = \frac{1}{D}(Q_2\bar{C}_{120} - Q_1\bar{C}_{110}) \quad (6)$$

where

$$D = \bar{C}_{110}\bar{C}_{220} - \bar{C}_{120}^2$$

When considering the symmetry of the function $H(\omega)$, the material is orthotropic, which in turn, implies

$$\bar{\alpha}_{120} = 0$$

The initial SMC properties are greatly influenced by its composition, mostly due to the anisotropy of the fiber bundle distribution and the inhomogeneity of the filler distribution. The TEPs as functions of varying mold coverage and "internal" filler fraction, characterized by the parameter Φ_{pi}, are shown in Figures 4 and 5, respectively.

RESIDUAL STRESSES

Due to a mismatch in thermoelastic properties of the laminate constituents (fiber bundles, resin compound, and filler), thermal stresses arise in the laminate structure while cooling from the elevated processing temperatures. These stresses are sufficiently large enough in SMC to influence the damage process, and thus cannot be neglected.

The SMC structure is modeled as an aggregate of UD plies; therefore, the state of stresses in these plies has to be analyzed. Consider the deformation of a ply oriented at an angle ω with the SMC orthotropic axis 0_1, as shown in Figure 2. The ply is firmly attached to all other UD plies within the SMC structure, implying that all plies undergo the same deformation when the SMC structure is di-

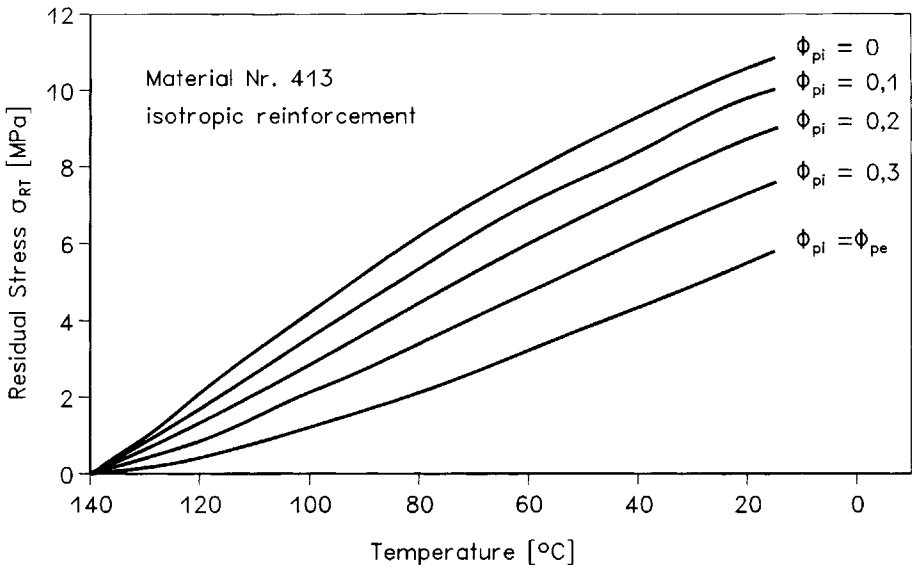

Figure 7 Development of the residual stress σ_{RT} with the cooling down for various filler fractions Φ_{pi}.

lated. Consider further that the TEP of components does not change within a temperature interval $\Delta T = T_2 - T_1$. The deformation of the laminate, caused by the temperature difference T, is then as follows:

$$\bar{\varepsilon}_1 = \Delta T \bar{\alpha}_{110}$$
$$\bar{\varepsilon}_2 = \Delta T \bar{\alpha}_{220}$$
$$\bar{\varepsilon}_{12} = 0 \qquad (7)$$

The free dilatation of the ply in question, in the direction of the local axes 0_L and 0_T, is given by

$$\varepsilon_L = \Delta T \alpha_L; \quad \varepsilon_T = \Delta T \alpha_T; \quad \varepsilon_{LT} = 0 \qquad (8)$$

By transforming the thermal strains defined in eq. (7) into the coordinate system defined by the 0_L and 0_T axes, the thermal stresses σ_{RL}, σ_{RT}, and σ_{RLT}, caused by the temperature difference ΔT in the ply, can be found as follows:

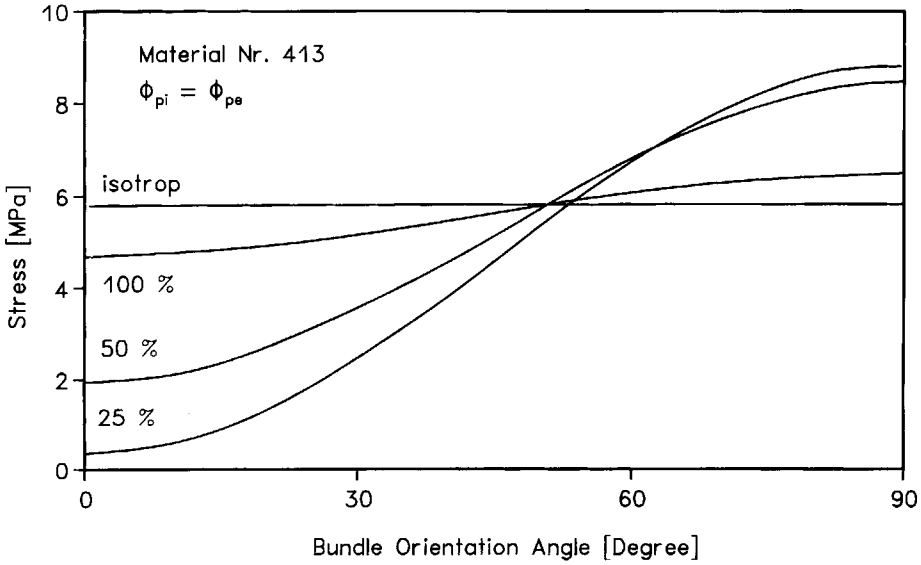

Figure 8 Residual stress σ_{RT} as a function of the mold coverage (corresponding to Fig. 3) and bundle orientation angle ω.

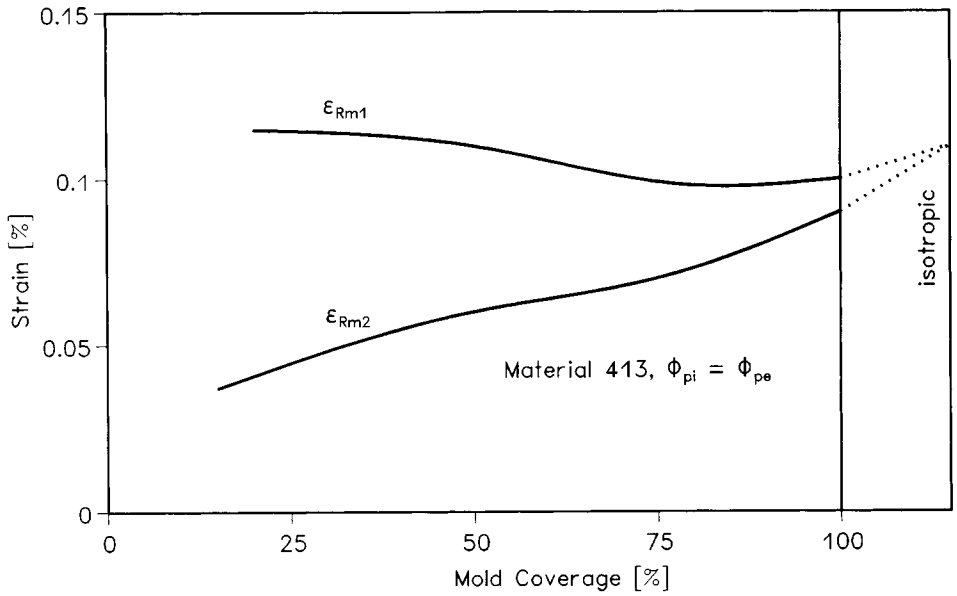

Figure 9 Residual matrix strains ε_{Rm1} and ε_{Rm2} in dependence on the degree of the fiber alignement.

$$\sigma_{RL} = (C_L \Delta\varepsilon_1 + C_{LT} \Delta\varepsilon_2)\Delta T$$
$$\sigma_{RT} = (C_{LT} \Delta\varepsilon_1 + C_T \Delta\varepsilon_2)\Delta T$$
$$\sigma_{RLT} = 2G_{LT} \Delta\varepsilon_{12} \Delta T \qquad (9)$$

where

$$\Delta\varepsilon_1 = \bar{\alpha}_1 m^2 + \bar{\alpha}_2 n^2 - \alpha_L$$
$$\Delta\varepsilon_2 = \bar{\alpha}_1 n^2 + \bar{\alpha}_2 m^2 - \alpha_T$$
$$\Delta\varepsilon_{12} = (\bar{\alpha}_1 - \bar{\alpha}_2) m \cdot n$$

and C_L, C_T, and C_{LT} are ply stiffnesses, G_{LT} the shear modulus and m = cos ω and n = sin ω.

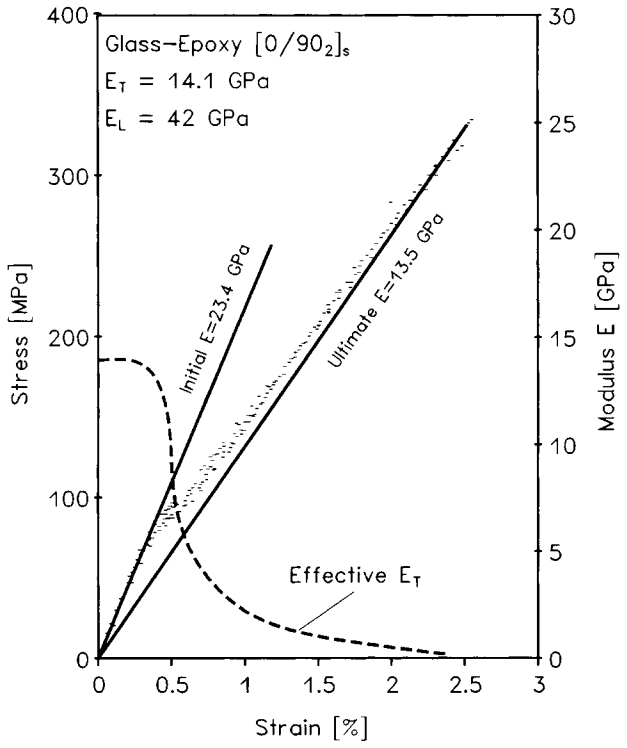

Figure 10 Stress–strain curve for a $[0/90_2]_s$ laminate.[6]

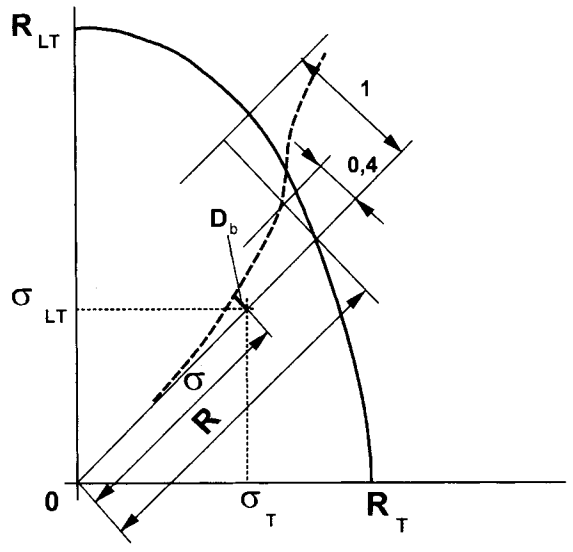

Figure 11 Definition of the parameters σ and R of the degradation function.[14]

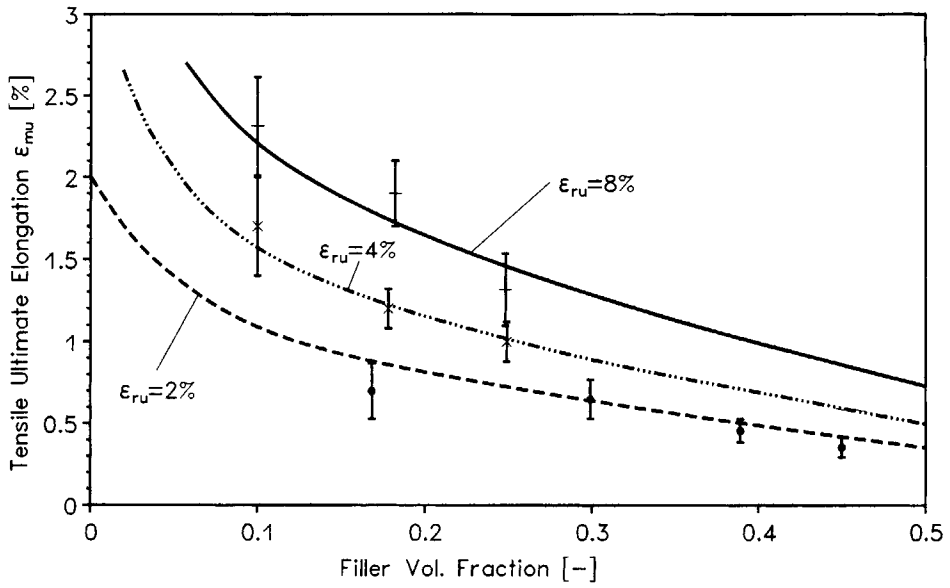

Figure 12 Dependence of the matrix ultimate tensile elongation ε_{mu} on the filler fraction Φ_{pe} and the resin tensile elongation ε_{ru}. Values of ε_{ru} (%) are indicated on the curves.

It is evident from eq. (9) that the thermal stresses are functions of the orientation angle ω. In the case when $\alpha_1 \neq \alpha_2$, a bundle orientation exists.

Along with the creation of the residual stresses in the fiber bundles, residual stresses also take place in the matrix (resin/filler mixture) that surrounds the bundle. It is assumed that the matrix deformation is planar and identical to the deformation of the laminate. The elastic strains arising in the matrix due to the temperature change of ΔT are thus:

$$\Delta\varepsilon_{m1} = (\overline{\alpha_{110}} - \alpha_m)\Delta T$$

$$\Delta\varepsilon_{m2} = (\overline{\alpha_{220}} - \alpha_m)\Delta T$$

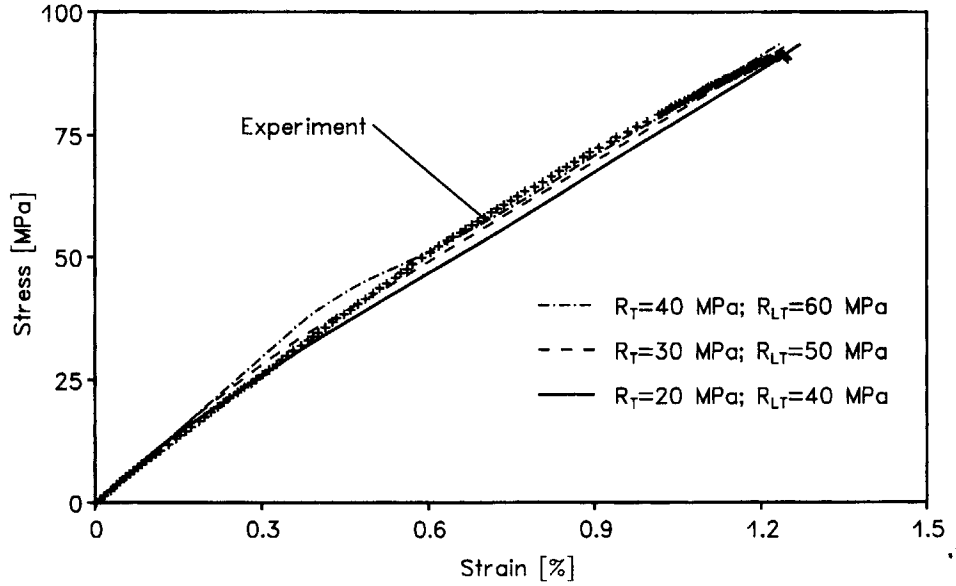

Figure 13 Experimental stress-strain curve for specimen No. 1 with predictions obtained for different values of strength R_T and R_{LT}.

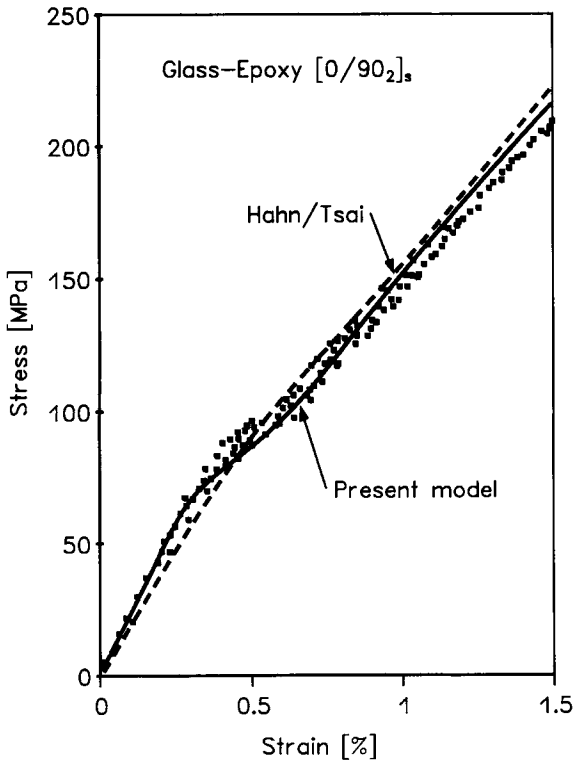

Figure 14 Predicted stress–strain curves for a cross-ply laminate[6] obtained on the basis of the Hahn/Tsai theory and the present model.

Assuming all properties to be constant within the temperature interval ΔT, the resulting residual stresses can be obtained as follows:

$$\sigma_{Rm1} = \frac{E_m}{1 - \nu_m^2} (\Delta\varepsilon_{m1} + \nu_m \Delta\varepsilon_{m2})$$

$$\sigma_{Rm2} = \frac{E_m}{1 - \nu_m^2} (\Delta\varepsilon_{m2} + \nu_m \Delta\varepsilon_{m1}) \qquad (10)$$

Because of the strong temperature dependency of all TEPs, the residual stresses depend not only on the value of the temperature differenceΔT, but also on the form of the temperature functions that represent the TEPs within the specific temperature interval. It can be assumed that TEPs of fibers and filler are constant up to a temperature of 200°C, and because processing temperatures rarely exceed 200°C, it is possible to calculate the temperature functions of all necessary composite characteristics when the temperature dependencies of the resin compound properties ($E_r(T)$, $\nu_r(T)$, and $\alpha_r(T)$) are known.

Because it was not possible to find these temperature dependencies throughout the entire processing temperature range, especially when approaching the temperature that ultimately leads to curing (about 140 to 150°C), it was necessary to extrapolate information from existing experimental results obtained at lower temperatures. The temperature functions used in the theoretical considerations are as follows:

$$E_r(T) = 1{,}57\left(\frac{\pi}{2} - \arctan\frac{T - 55}{35}\right) \quad [\text{GPa}]$$

$$\nu_r(T) = 0{,}064 \arctan\frac{T - 55}{64} + 0{,}4 \quad [-]$$

$$\alpha_r(T) = 12{,}5 \arctan\frac{T - 55}{32} + 74 \quad [10^{-6}\text{K}^{-1}] \qquad (11)$$

where T is substituted in °C.

The calculation of residual stresses is realized in small steps of ΔT. The final values of the stresses are obtained as a sum of individual stress increments. The graphical presentation of the functions in eq. (11) can be found in Figure 6, and the plots of residual stresses as functions of the structural parameter Φ_{pi} at various temperatures and of the fiber bundle alignment are shown in Figures 7 and 8, respectively. The influence of the fiber alignment on the matrix residual strains ε_{Rm1} and ε_{Rm2} can be seen in Figure 9. While the TEPs of SMC depend only slightly on the filler ratio Φ_{pi} (Fig. 5), its influence on the residual stresses is very substantial.

CRACKING MECHANISM

During the analysis of the cracking mechanism evidenced in SMC, it is assumed to be under the condition of a monotonically increasing tensile load acting along the direction of the 0_1 axis. It is also assumed that all plies are intact at the start of loading. The strength of a ply is a function of its orientation angle, and, thus, it can be expected that all plies will not fail at the same load. The extreme strength values of an UD ply are exhibited in the directions of the local 0_L and 0_T axes. A generally oriented lamina of our multilayer aggregate is subjected to a plane state of stressing defined by the stress components: σ_L, σ_T, and σ_{LT}. The stress σ_L is known to have a negligible effect on cracking along the fibers (within the matrix or along the fiber–matrix interface). Thus, the creation of these cracks depends only on σ_T and σ_{LT}.

Table I Thermoelastic Properties of SMC Constituents

			E Modulus [GPa]	Poisson's Ratio [−]	TEC [10^{-6} K^{-1}]	Tensile Elongation [%]
UP-resin	R1	Palatal A 420	3.4	0.38	60	2.3–4.0
	R2	Palatal P14	3.7	0.38	60	1.8–2.0
	R3	Palatal KR 51-22	3.4	0.39	60	2.5–4.0
	R4	Palatal KR 50-25	3.95	0.38	60	4
Filler	P1	Calcium carbonate upper fraction ≤ 3 μm	26	0.27	10	
	P2	Calcium carbonate upper fraction ≤ 5 μm	26	0.38	10	
	P3	Aluminum hydroxide upper fraction ≤ 2 μm	30	0.3	4	
	P4	Aluminum hydroxide upper fraction ≤ 8 μm	30	0.3	4	
Glass fiber	F1	Textile E-glass	70	0.25	5	2.4

The elliptic failure criterion is defined in the following form:

$$\frac{\sigma_T^2}{R_T^2} + \frac{\sigma_{LT}^2}{R_{LT}^2} = 1 \qquad (12)$$

where R_T and R_{LT} are tensile and shear strengths, respectively, determined experimentally. It is well known that a large scatter of data is an intrinsic characteristic of these measured strength quantities. This scatter is due to the complexity of the microdamage initiation and their sudden propagation. However, in a multilayer composite the local fracture propagates through the layer and causes a stress concentration in the still strong adjacent layer, which arrests its further propagation. Increasing the load will produce favorable conditions for creating new cracks in the same layer or at other locations. In this way, creation of statistically dispersed damage regions takes place, which in turn, causes degradation of some material properties—mainly the stiffness. A damaged ply cannot support any transverse tensile or shear load in the vicinity of the crack. Therefore, its contribution to the total stiffness is reduced. It becomes very difficult to ascertain the extent to which the effective stiffness of the laminae, and, ultimately, the total stiffness of the laminate, are influenced. Due to the statistical character of the crack initiation and propagation, an attempt has been made to evaluate the stiffness degradation on the basis of crack saturation—which is applied as a ply discount scheme.[15]

Consider a laminate subjected to the tensile stress σ_1 in the direction 0_1. The laminate strains then are:

$$\bar{\varepsilon}_1 = \frac{\sigma_1}{\bar{E}_1}; \quad \bar{\varepsilon}_2 = -\bar{\nu}_{12}\bar{\varepsilon}_1; \quad \bar{\varepsilon}_{12} = 0$$

A generally oriented lamina, defined by the angle ω, possesses strains identical to the laminate. After transforming these strains to the lamina local coordinate system 0_L and 0_T, the stresses σ_T and σ_{LT} acting on the lamina can be determined as follows:

$$\sigma_{LT} = G_{LT}\bar{\varepsilon}_1(1 - \bar{\nu}_{12})\sin 2\omega + \sigma_{RLT}$$

$$\sigma_T = \frac{E_T\bar{\varepsilon}_1}{1 - \nu_{LT}\nu_{TL}}((\nu_{LT} - \bar{\nu}_{12})\cos^2\omega - (\nu_{LT}\bar{\nu}_{12} - 1)\sin^2\omega) + \sigma_{RT} \qquad (13)$$

where σ_{RT} and σ_{RLT} are residual stresses.

When analyzing the initiation of cracking in a multilayer composite, the mean values of the strength quantities R_T and R_{LT} are usually substituted into the introduced failure criterion. The creation of initial cracks, nevertheless, takes place at a much lower load than that obtained by means of the failure criterion (e.g., as documented by AE measurements). This corresponds to the statistical character of these strength quantities. Several studies[6-10] have been carried out to establish experimentally, as well as theoretically, the quantitative influence resulting from the initiation and growth of cracks on laminate properties.

It was shown that the most frequent creation of cracks takes place at stresses near R_T or R_{LT}, which correlates with the maximum rate of stiffness reduction as found by Highsmith and Reifsnider.[9] A similar behavior can be deduced also from experi-

Table II Composition of the SMC Materials Investigated

Material Designation	Constituent			Constituent Volume Fraction		
	Fiber	Filler	Resin	v_f	v_p	v_r
1	F1	0	R1	0.208	0	0.792
96	F1	P3	R3	0.222	0.239	0.539
97	F1	P4	R3	0.222	0.239	0.539
98	F1	P4	R3	0.202	0.145	0.653
99	F1	P4[a]	R3	0.202	0.145	0.653
100	F1	P1[b]	R3	0.200	0.150	0.650
101	F1	P1	R2	0.200	0.150	0.650
413	F1	P1	R3	0.233	0.313	0.454
414	F1	P1	R3	0.233	0.313	0.454
416	F1	P1	R3	0.141	0.271	0.588
417	F1	P1	R3	0.220	0.246	0.534
420	F1	P1	R4	0.233	0.313	0.454
423	F1	P1	R3	0.200	0.150	0.650
429	F1	P1	R3	0.305	0.219	0.476
430	F1	P1	R3	0.243	0.363	0.394
436	F1	P1	R3	0.171	0.000	0.829
437	F1	P1	R3	0.220	0.246	0.534

[a] Methacryl-silan sizing.
[b] Fatty acid-ester sizing.

ments performed by Tsai and Hahn[6] on cross-ply laminates. On the basis of their results, shown in Figure 10, a curve describing the gradual reduction of the effective stiffness of the middle (cross oriented) layer was calculated. It can be seen in Figure 10, that the "knee," formed in the curve describing the behavior of E_T when the stress acting in the middle layer has reached the value R_T, coincides well with the largest rate of the stiffness reduction that has taken place. Many investigations dealing with the damage development in cross-ply laminates (e.g., [15]) show that a saturated state of cracking exists. This implies that the cracking rate approaches zero under a higher level of stressing. Thus, the de-

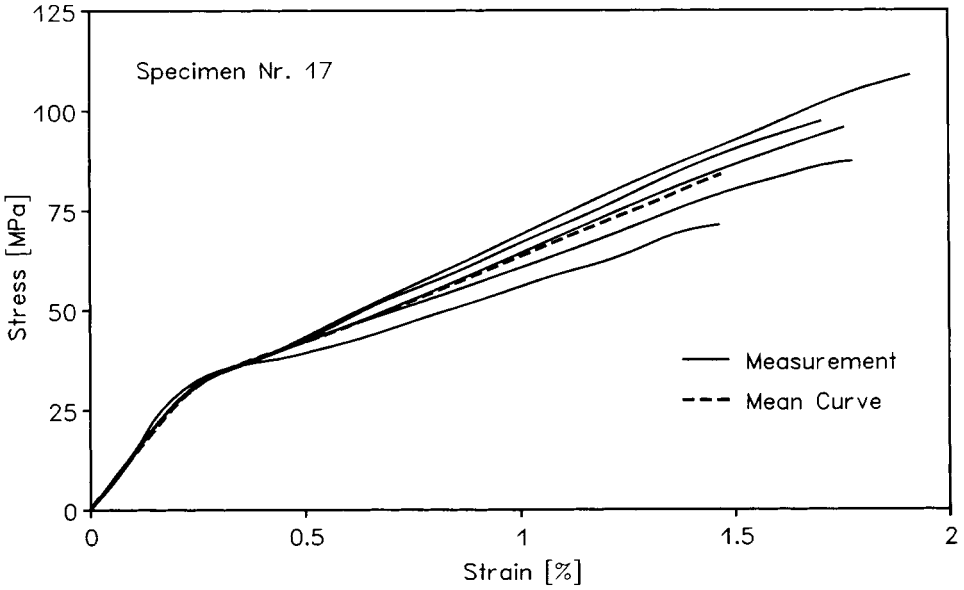

Figure 15 Plots of individual stress–strain curves (material No. 17).

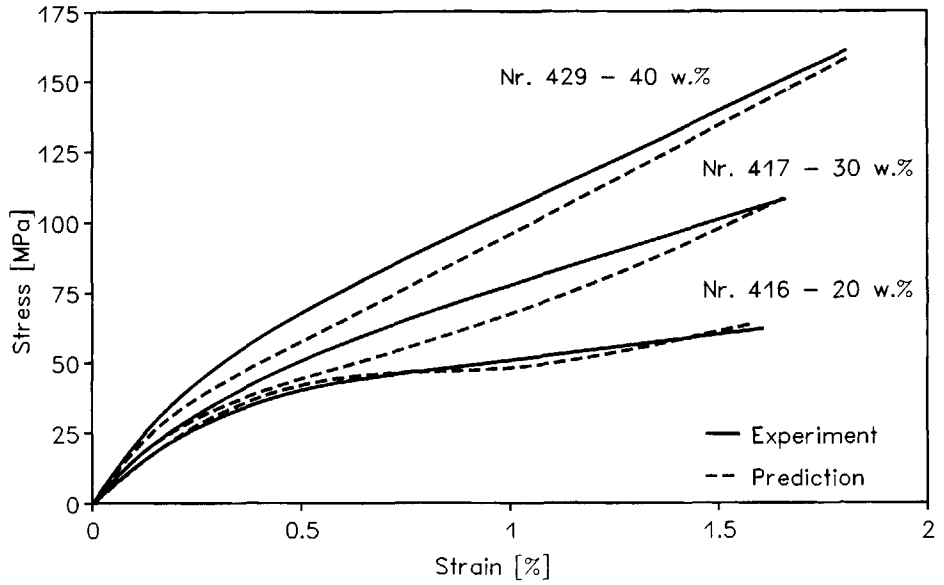

Figure 16 Comparison of the experimental and theoretical stress–strain plots for various fiber fractions.

rivative of the function used to describe the reduction of the middle layer stiffness has to approach zero at very low and high levels of stressing. At a stress equal to the strength, an inflexion point should exist in the function. These conditions are fulfilled by the following function:

$$D_b = 1 - e^{-a(\sigma/R)^{2b}} \tag{14}$$

where the following relation between positive constants a and b exists:

$$a = \frac{2b - 1}{2b}$$

The function D_b is defined through the constant b, which is significant for values of $b > 0.5$, and the strength quantity R, which has to be determined

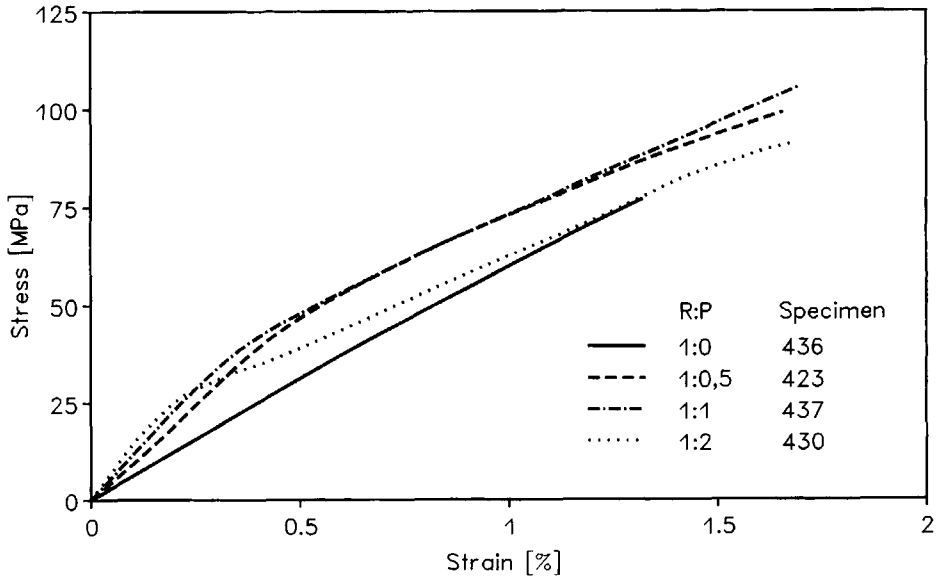

Figure 17 Effect of the resin-to-filler ratio on the stress–strain behavior of SMC—experimental results.

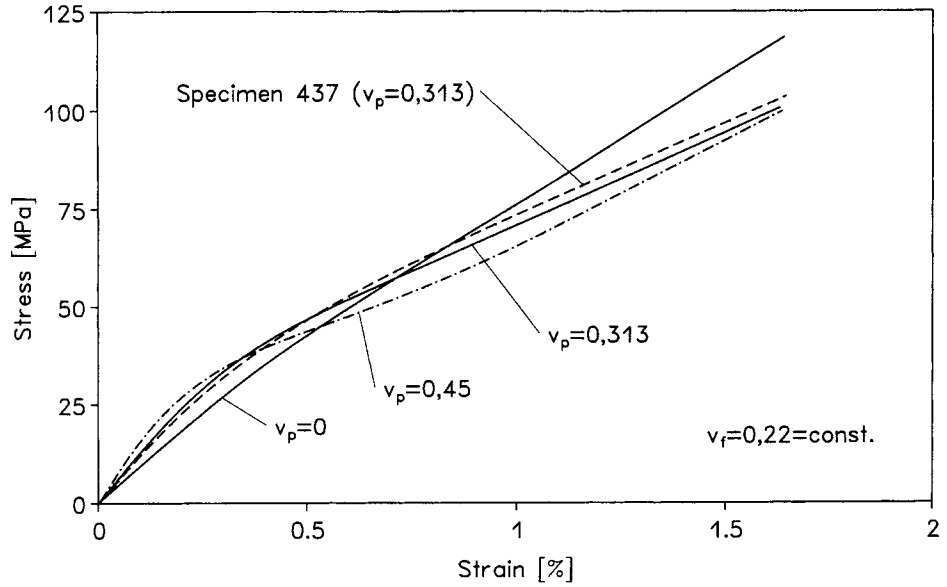

Figure 18 Predicted effect of resin-to-filler ratio on the stress–strain plots of sample No. 437, when volumen fiber fraction is constant (v_f = 0.22).

experimentally. However, the state of stressing of every ply is biaxial. Therefore, the quantities σ and R have to be defined on the basis of the acting stresses σ_T, σ_{LT}, and the strength values R_T and R_{LT}. With respect to the failure condition defined by eq. (12), the following expressions are substituted for σ and R:

$$\sigma^2 = \sigma_T^2 + \sigma_{LT}^2$$

$$R^2 = \frac{(\sigma_T^2 + \sigma_{LT}^2) R_T^2 R_{LT}^2}{\sigma_T^2 R_{LT}^2 + \sigma_{LT}^2 R_T^2}$$

The relationship between these quantities can be seen in Figure 11.

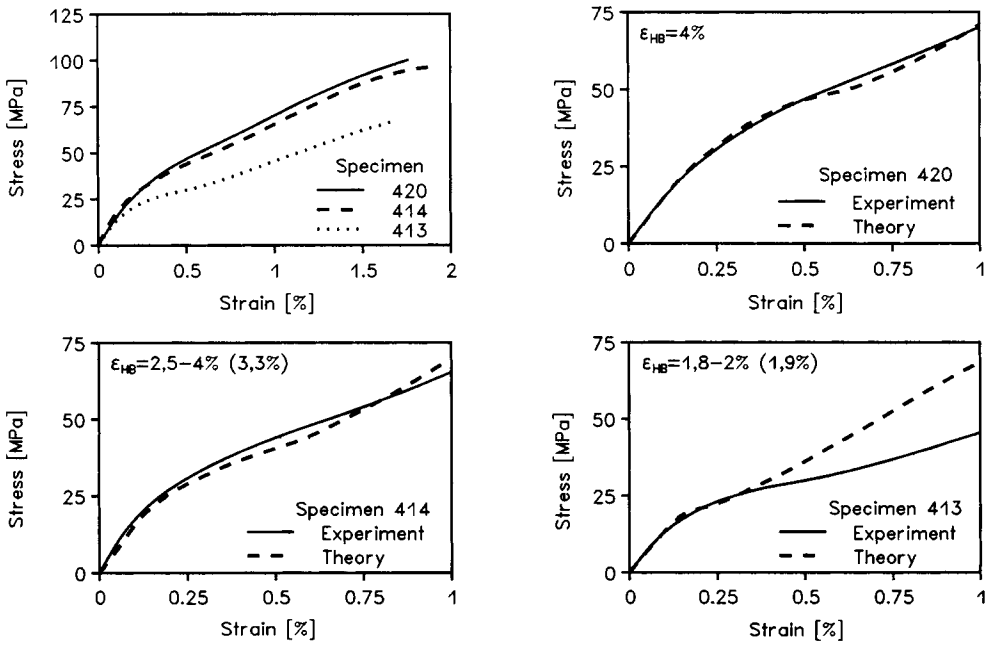

Figure 19 Experimental and predicted stress–strain plots when resins of different tensile elongation are applied.

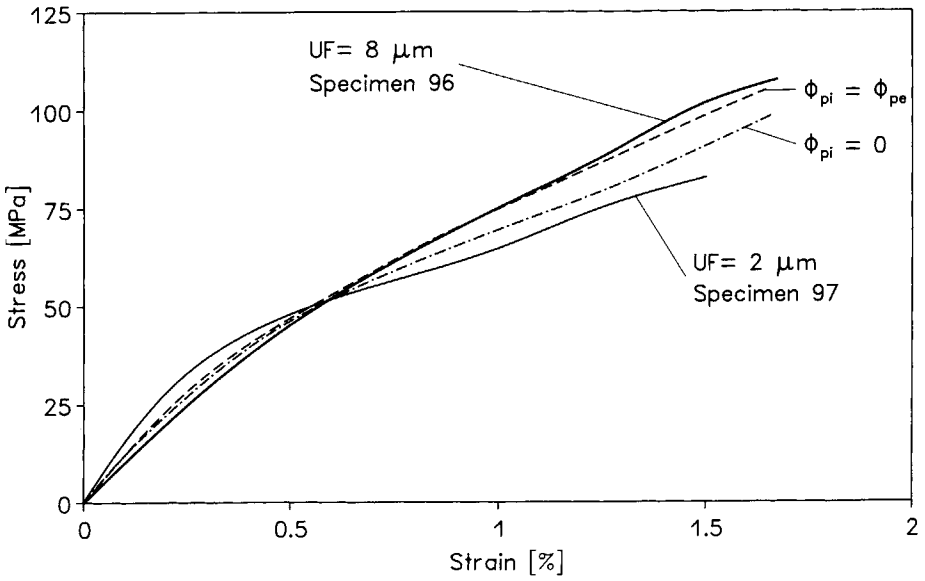

Figure 20 Influence of filler particles size distribution on SMC stress–strain plots.

As the fiber bundles start to crack, an initiation and propagation of cracks transversal to the loading direction also take place in the "external" matrix. The number of cracks, and in this way the reduction of the matrix contribution to the total laminate stiffness, is a function of the laminate deformation $\bar{\varepsilon}_1$. Similarly, as in the case of the bundles, the degradation function in the form of eq. (14) is used to describe the gradual reduction of the "external" matrix stiffness. The degradation function D_m is defined in terms of elongation:

$$D_m = 1 - e^{c(\varepsilon/\varepsilon_{mu})^{2d}} \tag{15}$$

where ε_{mu} is the matrix ultimate elongation, a and d are positive constants that fulfill the following relation:

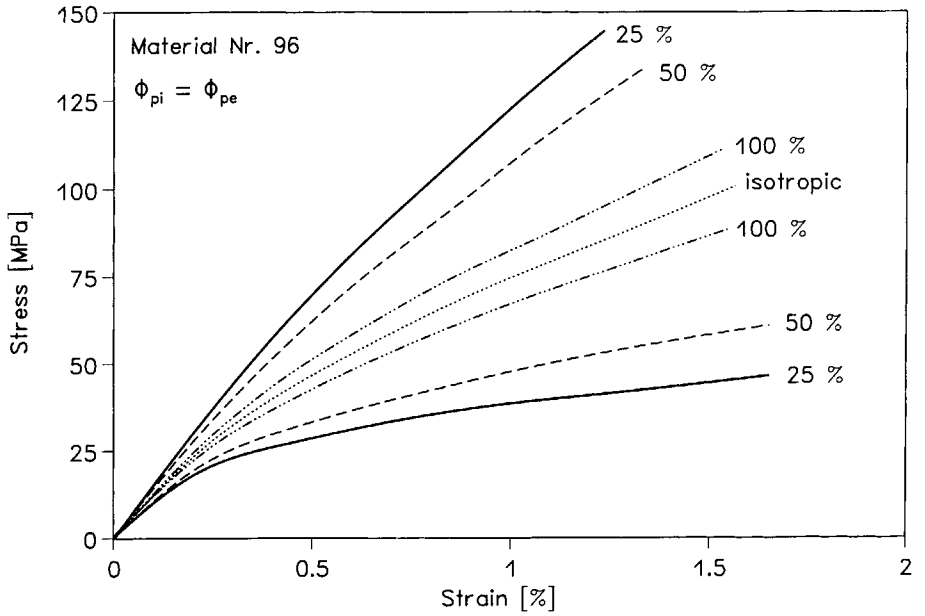

Figure 21 Stress–strain plots for different fiber alignements caused through the variation of the mold coverage corresponding to Figure 3.

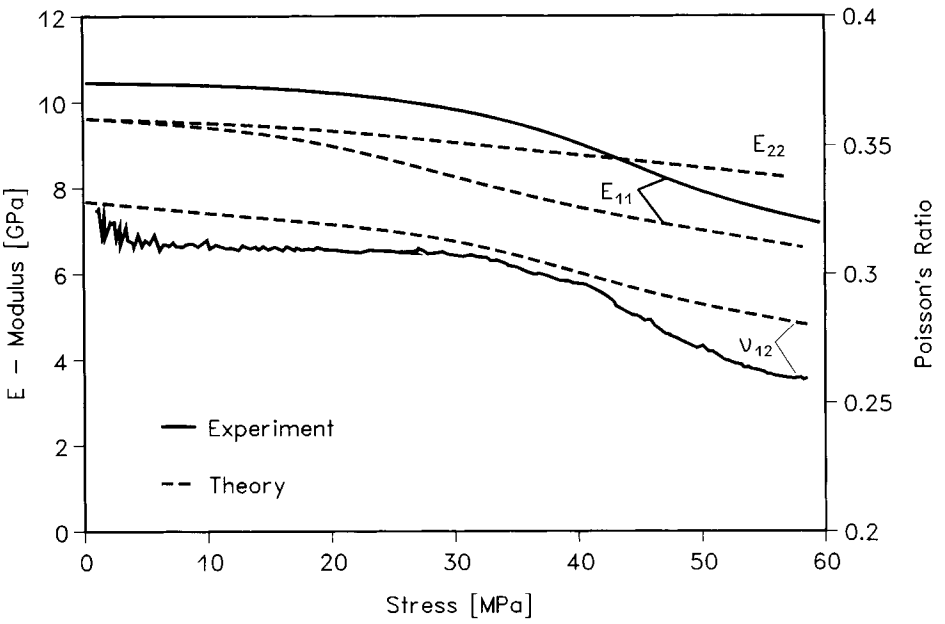

Figure 22 Reduction of the elasticity moduli E_{11}, E_{22}, and of the Poisson's ratio ν_{12} of SMC with increasing tensile stress.

$$c = \frac{2d - 1}{2d}$$

$$\varepsilon = \bar{\varepsilon}_1 + \varepsilon_{Rm1}$$

The matrix is subjected to the residual tensile strain ε_{Rm1}, which has to be added to the laminate deformation $\bar{\varepsilon}_1$.

The matrix ultimate elongation ε_{mu} surely depends in a very complicated way on the resin and filler properties, as well as on the filler volume fraction. Elongation test results, obtained on mixtures of calcium carbonate filler and resins at three different resin ultimate elongations, as shown in Figure 12, were used to develop the mathematical description for ε_{mu}. Thus, the elongation ε_{mu} was defined as a function of both filler fraction Φ_{pe} and resin ultimate elongation ε_{ru} as follows:

$$\varepsilon_{mu} = 1{,}5\sqrt{\varepsilon_{ru}}(1 - 1{,}04\sqrt[3]{\Phi_{pe}}) \qquad (16)$$

The cracks along the fibers reduce the transversal and shear stiffnesses of the individual layer, while its longitudinal stiffness remains unaffected. It is for this reason that the total laminate stiffness has to be reduced. The elements of the stiffness matrix corresponding to every level of the external load can be determined by applying the degradation function to the terms used to find the transversal and shear stiffnesses.

Similarly, the reduction of the matrix's ability to contribute to the total stiffness can be described by the reduction of the matrix shear stiffness and transverse tensile stiffness, with respect to the crack orientation, using the function D_m. Thus, the matrix starts to behave as an orthotropic material when cracks appear. The total SMC stiffness is then obtained as the sum of degradated stiffnesses, which are due to cracking of the individual plies.

The calculation of the σ-ε curve is performed through the use of a stepwise increasing elongation $\bar{\varepsilon}_1$. The actual stiffness values of the UD plies and the matrix layer are calculated at every step of loading, and the thermoelastic properties of the SMC are determined using the classical laminate theory. The corresponding stress $\bar{\sigma}_1$ is then assigned to every individual value of $\bar{\varepsilon}_1$, assuming that the SMC response is linear.

COMPARISON OF THE MODEL PREDICTIONS TO EXPERIMENTAL RESULTS

The accuracy of model predictions depends substantially on the correctness of data used in the calculations. The strengths R_T and R_{LT} are among the quantities that are of considerable importance when modeling the damage process that occurs in SMC. Very little data concerning glass fiber reinforced polyester resin was found in the literature.[11-13] The

experiments performed indicate that the SMC strength values are very sensitive to material inhomogeneities, as well as processing parameters (e.g., resin ductility, void content, fiber fraction, and surface treatment, residual stresses), which ultimately causes a large dispersion in the measured values. The measured data indicates that the R_T values lie within the interval of 12 to 32 MPa, while values for R_{LT} were determined to lie between 40 and 55 MPa. The mean value of the coefficients of variation, as a measure of dispersion, is about 15%. The measurements were carried out on specimens with fiber fractions greater 60% by volume, prepared by filament winding. However, in the case of SMC, the mean fiber fraction in bundles is about 50%. It was for these reasons that it was difficult to find appropriate strength values to use in the model. Thus, tensile tests were performed on specimens prepared of unsaturated polyester (UP) resin, reinforced by glass mat. The specimens were cured at a low temperature of 22°C, in order to keep thermal residual stresses to a minimum. Plots of the predicted stress–strain curves, at various values of R_T and R_{LT}, and experimental results are shown in Figure 13. It can be seen that a very good approximation can be obtained using the values R_T = 30 MPa and R_{LT} = 50 MPa. Thus, these strength values were applied in all further predictions.

A special investigation is necessary to determine the proper values of the parameters that appear in the degradation functions defined by eqs. (14) and (15). The values of b = d = 1 were used, on the basis of the preliminary tests, which are also in good agreement with the measurements of Hahn and Tsai,[6] as shown in Figure 14.

The experimental results obtained by Altstädt[4] in our laboratory were used to test the accuracy of the predictions. Altstädt examined the behavior of nearly 30 types of random sheet molding compound (R-SMC) materials; prepared of different combinations of resin (three types), glass fiber reinforcements (four types), filler (four types), and shrinkage compensators (two types). The properties of the individual constituents used are listed in Table I, and the compositions of the materials used in the investigations are listed in Table II.

The measurements were always performed using a set of six specimens; this was the basis for the determination of the mean stress–strain curves. A typical set of stress–strain curves for a specific SMC material, obtained through experimentation, is shown in Figure 15. It can easily be seen that a great deal of dispersion has occurred in the experimental results, especially at higher levels of loading. The stiffness and strength of the SMC specimens are highly influenced by the content (and orientation) of the reinforcing fibers. This is demonstrated in Figure 16, where the plots of stress–strain curves for three types of SMC specimens are compared. In these cases, reduction of the stiffness is somewhat moderated by the higher contents of filler used in specimens that possess lower fiber fractions.

The results of the investigation into the influence of resin-to-filler ratios, on stress–strain behavior, are presented in Figure 17. The predicted results, for the influence of the resin-to-filler ratios, are presented in Figure 18. It is very difficult to deduce the real influence that the resin-to-filler ratio has on the stress–strain relationship, because the curves obtained through measurement contain a certain amount of natural dispersion themselves. The specimens were prepared by keeping the weight fraction of fibers constant; consequently, the fiber volume fraction changed. Therefore, the prediction results presented in Figure 18 were calculated by holding the fiber volume fraction, v_f, constant at 0.22 (corresponding to the sample No. 437). By increasing the filler content, it is easily seen that the SMC stiffness increases. It can also be seen, that with an increasing filler content there is a greater tendency for a "knee" to form on the stress–strain curve.

The results of the investigations into the resin toughness effect for three SMC materials, along with the predicted curves, are shown in Figure 19. Both the experimental and theoretical stress–strain curves show the deformation behavior of SMC to be clearly influenced by resin toughness, especially at the onset of loading. Consequently, decreased resin toughness leads to lower stress values, which can be used as a limit to the linear stress–strain behavior. Once again, the tendency to form a "knee" on the stress–strain curve also becomes more obvious.

The influence of the filler particle size distribution can be seen in Figure 20. Two different size distributions of aluminum hydroxide were applied: a finer Apyral 40 with an upper fraction UF(50%) = 2 μm (implying that 50% of the particles are smaller than 2 μm) and an Apyral 4 with UF(50%) = 8 μm. The effect of particle size can be modeled into the prediction, assuming that the larger particles cannot penetrate into the bundles. This means that the fibers are wetted and attached by pure resin alone, in this extreme case. The plots corresponding to these cases can also be found in Figure 20. If the filler particles are large enough not to be able to penetrate into the bundles, then it can be expected that a more distinct "knee" is formed on the stress–strain curve at a lower load. The theoretical result is quite con-

tradictory to the experimental one. This could be due to a certain alignment of the reinforcing fibers, which is substantiated by the difference between the initial moduli. The influence of fiber alignment, for various levels of material anisotropy, on the SMC damage process can be seen on Figure 21.

The creation of cracks in the bundles, as well as in the matrix, is directionally dependent. The cracks in the "external" matrix are mostly transversally oriented to the load. The transversally oriented bundles also offer the best conditions for cracking. Therefore, the behavior of SMC becomes orthotropic in nature, or the degree of initial anisotropy changes as the cracks develop. This phenomena can be seen in Figure 22, where the variation of the elasticity moduli E_{11}, E_{22}, and Poisson's ratio $\overline{\nu_{12}}$ for both experimental and predicted results, are presented for increasing levels of stress.

SUMMARY AND CONCLUSIONS

A comparison of prediction to the experimental results shows that the developed model is able to describe the behavior of the SMC under tensile loading very well, especially at lower levels of the loading phase. When a higher level of crack density is reached, the damage process gradually becomes of a local character, which the model is not able to take into account. Substantial differences seen between the experimental and theoretical curves, during the second half of the loading cycle, could also be due to the initial anisotropy of the investigated SMC samples, while the prediction results were mostly carried out assuming that the SMC was isotropic. To prevent the misrepresentation of results due to the material anisotropy, generally, it is necessary to cut the measurement specimens in two mutually perpendicular directions.

The model involves the influence of many material parameters, as well as processing parameters, which allows the quantitative evaluation of the influence of these individual parameters on the SMC damage process. Ultimately, this model can be used to optimize the SMC properties. Based on this work, the following general conclusions can be reached:

1. The behavior of SMC is substantially influenced by the distribution of the filler particles. Optimal SMC behavior can be expected when fine enough particles are applied, and a homogeneous distribution throughout the entire SMC volume is ensured.
2. The residual stresses (σ_{RT}) acting in the transversal fiber direction within the bundles and in the matrix (σ_{Rm1}, σ_{Rm2}) are tensile in character and can reach a level that is comparable to the local material strength values. Reducing the residual stresses seems to be a very promising way for improving the application limits of SMC.
3. The first cracks usually take place as a consequence of stresses acting in the fiber bundles. When a rough filler in higher fractions is applied, the most favorable conditions for crack initiation can arise in the matrix.
4. The crack resistance is governed by the resin properties, especially by their toughness and adhesion ability. The tensile stiffness of SMC is governed by the fiber content. Therefore, a small loss in stiffness—when a more ductile and lower elasticity modulus resin is applied—could be balanced by slightly enhancing the fiber fraction.
5. The creation of cracks is directionally dependent. The stiffness loss rate is higher in the loading direction than in the transversal one. Consequently, SMC behavior becomes anisotropic in nature as the damage process proceeds, and in addition this level of anisotropy is increased further if the SMC material is initially anisotropic in nature.

The model developed in this work is based on the assumption that SMC, as well as all its constituents, behave in a linear elastic way. In spite of this simplification, and an incomplete knowledge of much of the other necessary data, encouraging results were obtained. Thus, it appears that further investigation in this area will provide a very useful tool in understanding the complexity of SMC materials and in their applications.

REFERENCES

1. J. Kabelka and G. W. Ehrenstein, *Structure and Thermo-Elastic Properties of SMC*, 47th Annual Conference, CI SPI, Cincinnati, 1992, Sess. 1-E.
2. Z. Hashin, *J. Appl. Mech.*, **46,** 543 (1979).
3. Z. Hashin, *J. Appl. Mech.*, **29,** 143 (1962).
4. R. L. Mc Coullough and S. M. Whitney, *Micromechanical Materials Modelling, Delaware Composites Design Encyclopedia*, Vol. 2, Technomic Pub. Co., Lancaster, PA, 1990.
5. V. C. Halpin, *Primer on Composite Materials: Analysis*, Technonomic, Stanford, CT, 1984.
6. H. T. Hahn and S. W. Tsai, *J. Comp. Mater.*, **8**(3), 288 (1974).

7. S. C. Chou, O. Oringer and J. H. Rainey, *J. Comp. Mater.*, **10**(4), 371 (1976).
8. T. R. Porter, in *Fatigue of Filamentary Composite Materials,* K. L. Reifsnider and K. N. Lauraitis, Eds., STP 636, ASTM, Philadelphia, PA, 1977.
9. A. L. Highsmith, K. L. Reifsnider, in *Damage in Comp. Material,* K. L. Reifsnider, Ed., ASTM STP 775, Philadelphia, PA, 1982.
10. G. Zhanjun and K. L. Reifsnider, in *Composites Materials Fatigue and Fracture,* Vol. 4, K. L. Reifsnider, Ed., ASTM STP 1156, Philadelphia, PA, 1883, p. 453.
11. W. Knappe and W. Schneider, *Kunststoffe,* **62**(12), 864 (1972).
12. J. Kabelka and J. Vejchar, Zur Problematik der Festigkeit unidirektional verstärkter Kunststoffe, Proc. AVK-Conference, Freudenstadt, 1972, p. 14–1.
13. J. Padovec and J. Zenahlik, Proc. Verstärkte Plaste '84, Berlin, 1984, Kammer der Technik H2.
14. V. Altstädt, Dissertation, Universität Kassel (GH), D, 1984.
15. R. Talreja, *J. Strain Anal.,* **24**(4), 27–34 (1989).
16. J. Starke and W. Michaeli, Proc. 25th Int. AVK Conference, Berlin, 1993, P4/1–8.

Received April 26, 1995
Accepted April 22, 1996